Determination of the Rate Constants for the NCO($X^2\Pi$) + Cl(^2P) and Cl(^2P) + ClNCO(X^1A') Reactions at 293 and 345 K

Yide Gao[†] and R. Glen Macdonald*

Chemistry Division, Argonne National Laboratory, 9700 South Cass Avenue, Argonne, Illinois 60439-4831

Received: February 2, 2005

The rate constant for the reaction of the isocyanato radical, NCO($X^2\Pi$) with chlorine atoms, Cl(^2P), has been measured at 293 ± 2 and 345 ± 3 K to be (6.9 ± 3.8) × 10^{-11} and (4.0 ± 2.2) × 10^{-11} cm^3 molecules^{-1} s,$^{-1}$ respectively, where the uncertainties include both random and systematic errors. The measurements were carried out at pressures of 1.3−6.2 Torr with either Ar or CF_4 as the bath gas and were independent of both pressure and nature of the third body. Equal concentrations of NCO and Cl atoms were created by 248 nm photolysis of ClNCO. The reaction was monitored by following the temporal dependence of NCO($X^2\Pi$) using time-resolved infrared absorption spectroscopy on rotational transitions of the NCO(10^01) ← (00^10) combination band. The reaction rate constant was determined by using a simple chemical model and minimizing the sum of the residuals between the experimental and computer generated temporal NCO concentration profiles. The reaction Cl + ClNCO → Cl_2 + NCO was found to contribute to the observed NCO. The rate constant for this reaction was found to be (2.4 ± 1.6) × 10^{-13} and (1.9 ± 1.2) × 10^{-13} cm^3 molecules^{-1} s,$^{-1}$ at 293 and 345 K, respectively, where the uncertainties include both random and systematic error.

I. Introduction

The NCO radical is an important intermediate in combustion systems.[1] It is the link between fuel-fixed nitrogen compounds and their ultimate fate forming NO_X species. As well, the NCO radical contributes to NO_X formation by the so-called prompt NO_X or Fenimore mechanism. This chemistry is initiated by the reaction of simple hydrocarbon radicals such as CH and $^3CH_2$ with N_2 and occurs at low flame temperatures. Furthermore, the NCO radical plays an important role in several NO_X abatement strategies involving the addition of various chemicals to flue gases.[2] As an example, the RAPRENOx process uses cyanuric acid, $(HOCN)_3$, addition to efficiently remove NO_X from flue gases. At the temperature of the flue gas, the cyanuric acid is converted to HNCO, which is then oxidized to generate the NCO radical. Subsequent chemistry involving the NCO radical, primarily NCO + NO, removes NO from the flue gas.

Atom−radical and radical−radical reactions play a unique role in many chemical processes. They can be chain propagating or termination reactions depending on the product channels of the reaction.[3] Furthermore, radical−radical reactions are always governed by multiple potential energy surfaces, PESs. If the reactant atom or radical possesses electronic angular momentum, there are multiple electronic surfaces as well as multiple spin manifolds. The presence of multiple electronic and spin manifolds gives rise to the question as to the influence on the reaction dynamics of the coupling between either electronic states, i.e., internal conversion, IC, or between spin manifolds, i.e., intersystem crossing, ISC.[4] Theoretical descriptions of these curve crossing processes are becoming increasingly more accurate.[5]

The present work involves the study of the radical−atom reaction

$$NCO(X^2\Pi) + Cl(^2P_u) \rightarrow NCl(X^3\Sigma^-) + CO(X^1\Sigma^+) \quad \Delta H_{r,0} = -36 \text{ kJ mol}^{-1} \quad (1)$$

The reaction exothermicity, $\Delta H_{r,0}$, was calculated using a recent recommendation for the heat of formation of NCO at 0 K, $\Delta H^0_{f,0}$(NCO), of 128 ± 0.8 kJ mol^{-1} based largely on high level theoretical calculations[6] and the $\Delta H^0_{f,0}$(NCl) of 325 ± 5 kJ mol^{-1}, also based on high level theoretical calculations.[7]

Both NCO and Cl possess electronic angular momentum so that there are 3($^1A'$+ $^1A''$) and 3($^3A'$ + $^3A''$) PESs correlating to the reactants in planar C_s symmetry. If the products are as written, they correlate to the lowest energetic triplet PES, a^3A''. ISC could play an important role in the collision dynamics if the initial interaction between NCO and Cl occurs on the lowest energetic PES, the ClNCO(X^1A').

The NCO and N_3 radicals are isoelectronic and are expected to undergo similar reaction dynamics. The more characterized $N_3(X^2\Pi)$ + Cl(^2P) → NCl($X^3\Sigma^-$)/NCl($a^1\Delta$) + $N_2(X^1\Sigma^+)$ can be used to understand some of the reaction dynamics for reaction 1, for which there are no previous measurements. The N_3 + Cl reaction system has received considerable more attention because of the potential to construct a high power chemical laser based on the electronic energy transfer between NCl($a^1\Delta$) and the spin−orbit states of the I atom.[8]

Reaction 1 was initiated by photodissociation of ClNCO at 248 nm to create equal concentrations of NCO radicals and Cl atoms. The temporal dependence of the NCO radical was followed using time-resolved infrared absorption spectroscopy using rotational transitions of the NCO($X^2\Pi$) (10^01) ← (00^10) combination vibration band near 3.15 μm. A simple kinetic model was constructed and the calculated NCO concentration profiles were compared to the experimental measurements. The optimum value of k_1 was determined by minimizing the sum of the squares of the residuals between the model predictions and the experimental NCO profiles. The reaction Cl + ClNCO

* To whom correspondence should be addressed. E-mail: rgmacdonald@anl.gov. Fax: (630) 252−9292.

[†] Current address: Department of Chemistry, University of North Texas, P.O. Box 305070, Denton, TX 76203-5070.

10.1021/jp058038r CCC: $30.25
Published on Web 05/28/2005

$\rightarrow$ NCO + Cl_2 was observed to contribute to the formation of NCO and its rate constant was determined in the data analysis as well.

II. Experiment

The experimental apparatus[9] has been described previously so only a brief description is given here. The rectangular stainless steel reaction chamber contained an inner Teflon box with dimensions 100 × 100 × 5 cm that could be heated from 290 to 390 K using a Nestlab EX-250HT recirculating oil bath. The reaction chamber was evacuated to a base pressure of 5×10^{-6} Torr and had a leak rate of about 5×10^{-4} Torr min.$^{-1}$ Known flows of the various gases were admitted to the reaction chamber from separate vacuum systems using calibrated electronic flow meters. Both the Ar and CF_4 gases were supplied by AGA and were 99.995 and 99.9% pure, respectively. The gases were used directly from the cylinders.

A constant flow of the transient ClNCO molecule was created by a slight modification of the thermolysis procedure suggested by Nachbaur and Gottardi.[10] The ClNCO generator consisted of two heated regions: one containing the polymeric form of ClNCO, $(ClNCO)_3$, was heated to about 410 K to create $(ClNCO)_3$ vapor, and the other, was heated to about 550 K to thermally dissociate $(ClNCO)_3$ to ClNCO. A measured flow of Ar (20−30 sccm) was passed continuously through the ClNCO generator. The total pressure in the generator was monitored by a pressure transducer. The concentration of ClNCO, [ClNCO] (the square brackets will be used to indicate concentration in molecules cm^{-3} throughout), in the reaction chamber could be varied by changing the Ar flow through the generator and/or the temperature of the $(ClNCO)_3$ reservoir.

The ClNCO could be admitted to the reaction chamber through two ports: the first, 1.0 cm upstream from the photolysis zone and the second 22 cm upstream. There was no detectable difference in the results obtained using either port. The flow rate of ClNCO was small and could not be measured reliably by measuring the pressure change in the generator when the Ar flow by-passed the heated zones. However, the absorption cross section[11] of ClNCO at 248 nm has been measured to be 1.8×10^{-18} cm^{-2} molecules.$^{-1}$ The [ClNCO] in the reactor was determined by measuring the attenuation of the KrF photolysis laser intensity when ClNCO was admitted to the reaction chamber or when the Ar flow by-passed the heated zones of the ClNCO generator. A second method for determination of the [ClNCO] was based on the pressure decrease in the reaction chamber when the Ar flow by-passed the heated zones of the generator, thus removing most of the ClNCO from the Ar flow. Both techniques for the determinations of [ClNCO] were in agreement with each other to within about ±20%. Generally, both methods were used to measure the [ClNCO] several times during an experiment and a simple average taken.

The photolysis laser was a Lamda-Physik Compex 205 excimer laser operating at 248 nm at a repetition rate of 1−3 Hz. This repetition rate ensured that a fresh sample of gas was photolyzed on each laser pulse. Part of the photolysis laser beam was transmitted through the reaction vessel and monitored by a power meter. The [ClNCO] was kept low enough so that the attenuation of the photolysis laser intensity was always less than 20% and generally around 10%. The nominal photolysis laser fluence at the entrance window of the reaction chamber was varied between 3 and 25 mJ cm.$^{-2}$ The excimer laser was operated in a constant energy mode. To achieve low fluence laser pulses with reduced pulse-to-pulse fluctuations, the KrF laser was operated at maximum power and attenuated by fine stainless steel screens.

The temporal dependence of the [NCO($X^2\Pi(00^10)$] radical was monitored by the $P_{1e/1f}(12.5)$ transition of the $(10^11) \leftarrow (00^10)$ combination band using the output of a Burleigh Model 20 single-mode color-center laser. The probe and photolysis laser beams were spatially overlapped using an UV−IR dichroic mirror set at Brewster's angle on the optical axis of the White cell. A ZnS plate, also placed at Brewster's angle on the White cell axis, protected the opposite White cell mirrors from the photolysis laser beam and deflected part of the photolysis beam out of the reaction chamber onto the power meter that monitored the excimer laser intensity. The distance between these two optical elements, 139 cm, defined the optical path length of the probe laser. Most of the data were recorded for twelve passes of the probe laser through the photolysis zone.

The largest source of noise in the experiments was due to amplitude fluctuations of the infrared laser. To minimize this noise source several steps were taken. The probe laser beam was split into two beams and monitored by separate identical InSb infrared detectors. The signals from both detectors were equalized using infrared polarizers. The signal from the detector that monitored the initial probe laser intensity, I_0, was sent to a ConOptics model Lass-II noise eater. The noise eater modulated the intensity of the Kr^+ laser pumping the color center laser and compensated for amplitude variations of the infrared laser beam. Further noise reduction was accomplished by using a dc differential amplifier to process the difference signal between the balanced I_0 and I signals. The difference signals were recorded and signal averaged using a LeCroy 9410 digital oscilloscope operating in the DC mode. The I_0 signal was measured by sampling the output of a boxcar integrator triggered 1 ms before the excimer laser fired. The data collection was under the control of a laboratory computer.

III. Results

A. Concentration Determination. The infrared probe laser bandwidth is much narrower than the Doppler width of the NCO $P_{e/f}(12.5)$ absorption feature so that the Beer−Lambert law[12] can be used to directly relate absorbance at frequency ν and time t, $A(\nu,t)$, to the concentration of NCO, [NCO(t)]

$$A(\nu,t) = \ln(I_0(\nu)/I(\nu)) = l\sigma_{pk}(\nu)[\mathrm{NCO}(t)] \qquad \text{(E1)}$$

$I_0(\nu)$ and $I(\nu)$ are the initial and transmitted probe laser intensity at frequency ν, respectively, l is the path length, and $\sigma_{pk}(\nu)$ is the peak absorption coefficient for the monitored absorption feature.

In using eq E1, one assumes that the NCO vibrational manifold is in thermal equilibrium with the ambient temperature of the reaction chamber. An initial nonequilibrium NCO vibrational distribution can result in an incorrect determination of [NCO(t)], and its influence on the experiments needs to be addressed as only the ground-state vibrational level could be monitored. The 248 nm photodissociation of ClNCO leaves an estimated 270 kJ mol^{-1} of energy (see section III.C) to be partitioned between relative translational energy of the fragments and the internal energy of NCO. Fortunately, several factors reduce the possibility that vibrationally excited NCO significantly influenced the present measurements. First, an absorption measurement always measures the degeneracy-weighted population difference between the two quantum states connected by the radiative transition.[12] For the 248 nm photolysis of ClNCO, there was sufficient excess energy to directly populate the NCO-(10^11) vibrational level; however, there was no experimental evidence for a population inversion between the NCO(10^11) and

(00^10) vibrational levels. A population inversion would have been indicated by a negative absorption signal at the beginning of the NCO absorption profiles. The infrared detectors had a frequency response of about 5 MHz so that the initial rise in the NCO absorption signals were temporally well-resolved. Second, the photodissociation of ClNCO likely takes place on a repulsive potential energy surface, leading to relative translational motion receiving the largest fraction of the energy release. Third and most importantly, the vibrational relaxation[13] of NCO, particularly the bending modes, has been found to be fast even for inert gas collision partners; e.g., the rate constant for removal of NCO(01^20) bending levels by Ar has been measured[14] to be 4.7×10^{-13} cm^3 molecules^{-1} s.$^{-1}$ More highly excited levels are expected to be removed with even larger rate constants[15] so that even at the lowest pressures used in the present work at most an induction time of only a few 10's of microseconds could be anticipated compared to reaction times of a few milliseconds. The only difference between NCO absorption signals obtained with CF_4 or Ar as bath gas was that the peak in the NCO signal occurred slightly earlier in time with CF_4, indicating more efficient energy transfer by CF_4. In any case, to account for a possible small induction period due to vibrational relaxation, the NCO temporal concentration profiles were not analyzed for the first 50 μs.

Almost all the data reported here were collected using the NCO(10^11) $P_{e/f}(12.5)$ transition. For this low J transition the Λ-doubling splitting in NCO cannot be resolved, but the splitting is estimated to be smaller than the Doppler width at 293 K.[16] Other experiments in this laboratory prompted a new determination of the absorption coefficient for this transition. The new measurement gives σ_{pk} to be $(3.22 \pm 0.24) \times 10^{-19}$ cm^2 molecules^{-1} at 293 K, which is 8.0% smaller than our previous measurement[17] but within the experimental uncertainty. At 345 K, the peak absorption coefficient for this transition was calculated to be 2.2×10^{-19} cm^2 molecule.$^{-1}$ This calculation accounted for the change in Doppler width with temperature and used an exact vibrational partition function to calculate population changes with temperature. The NCO vibrational energy levels observed by Patel-Misra et al.[18] were used to calculate the vibrational partition function, explicitly accounting for the influence of the Renner−Teller effect.

B. Reaction Mechanism. The following reaction mechanism describes the NCO production and removal processes following the 248 nm photolysis of ClNCO:

$$\mathrm{ClNCO} \xrightarrow{248\ \mathrm{nm}} \mathrm{NCO}(X^2\Pi) + \mathrm{Cl}(^2\mathrm{P}) \quad (2)$$

$$\mathrm{NCO} + \mathrm{Cl} \rightarrow \mathrm{NCl}(X^3\Sigma^-) + \mathrm{CO} \quad (1)$$

$$\mathrm{NCO} + \mathrm{NCO} \rightarrow \mathrm{N_2} + 2\mathrm{CO} \quad (3)$$

$$\mathrm{NCl} + \mathrm{NCl} \rightarrow \mathrm{N_2} + 2\mathrm{Cl} \quad (4)$$

$$\mathrm{Cl} + \mathrm{ClNCO} \rightarrow \mathrm{NCO} + \mathrm{Cl_2} \quad (5)$$

$$\mathrm{Cl} + \mathrm{Cl} + \mathrm{M} \rightarrow \mathrm{Cl_2} + \mathrm{M} \quad (6)$$

$$\mathrm{NCO} \xrightarrow{k_{\mathrm{diffusion}}} \mathrm{NCO} \quad (7)$$

The photodissociation of ClNCO has been studied by Coombe and co-workers;[11,19] however, the quantum yield for the photolysis products of ClNCO has not been determined. It is possible that a molecular channel producing NCl + CO contributes to the product yield, but there is strong experimental evidence that this contribution is small or negligible. At 248 nm there is sufficient energy available to populate the NCl singlet state, which would be the major product in an allowed electronic transition; however, Bell and Coombe did not detect any NCl($a^1\Delta$) → ($X^3\Sigma$) emission, indicating that there was little or no NCl($a^1\Delta$) generated in the photodissociation process. It is unlikely that intersystem crossing could convert all the initial NCl($a^1\Delta$) to ($X^3\Sigma$), and some NCl($a^1\Delta$) → ($X^3\Sigma$) emission should have been detected if the NCl + CO product channel were significant. The [NCO] calculated from the attenuation of the photolysis laser and the measured ClNCO absorption coefficient[11] agreed with the measured [NCO] assuming NCO + Cl was the only channel in the photodissociation. Although, as noted in section II, there was some uncertainty in the determination of the [ClNCO]. Furthermore, in experiments in this laboratory,[20] the reaction Cl + CH_4 → CH_3 + HCl was used to study the NCO + CH_3 reaction. All three species, NCO, CH_3, and HCl, were monitored, and their concentrations were consistent with NCO + Cl being the only product channel in the photodissociation of ClNCO. If the NCl + CO channel were important, an excess of HCl over NCO would have been observed due to reaction 4.

The rate constant for reaction 3 has been measured by Wategaonkar and Setser[21] to be $(5.0 \pm 2.0) \times 10^{-12}$ cm^3 molecule^{-1} s^{-1} at 298 K. The products for this reaction were not directly identified by these authors but N_2 and 2CO were assumed the most likely, given the large exothermicity for this product channel. The rate constant for reaction 4 has been measured by Clyne and MacRobert[22] to be $(8.1 \pm 1.8) \times 10^{-12}$ cm^3 molecule^{-1} s^{-1} at 295 K. Similarly, the products of reaction 4 were not directly identified but the author's suggest that the reaction likely proceeds by the formation of a transient complex, N_2Cl, and Cl, with subsequent fragmentation of the complex to N_2 and Cl, similar to the disproportionation reaction between two NF radicals.[23] Reaction 5 was needed to account for the observed production of NCO at long times and was determined in the data analysis. The rate constant for the recombination of two Cl atoms, reaction 6, was taken as $(1.13 \pm 0.23) \times 10^{-32}$ cm^6 molecules^{-2} s^{-1}, independent of the nature of the third body.[24]

The only species that could be monitored in the present experiments was the NCO radical so that the rate constant describing loss by diffusion, $k_{\mathrm{diff}}^{\mathrm{NCO}}$, could not be directly determined. However, this laboratory has acquired a great deal of information of the loss of HCN by diffusion in both Ar and CF_4 under similar experimental conditions, particularly at 293 K, and these measurements were used to estimate the first-order rate constant for loss by diffusion, $k_{\mathrm{diff}}^{\mathrm{X}}$, for each species, X, in the reaction system. As a first approximation to a binary diffusion constant,[25] gas kinetic theory gives the binary diffusion constant to be proportional to $T^{1.5}$ and inversely proportional to the product of the pressure, the square of the collision cross section, and square root of the reduced mass. The diffusional loss rate constant is the product of the binary diffusion constant and a geometrical factor describing the boundary conditions of the experiment[26] (a rectangular parallelepiped under the present conditions). Simple gas kinetic binary diffusion constants were calculated for each species in the system, using tabulated[27] Lennard-Jones cross sections and divided by that for HCN. This ratio was then multiplied by the experimentally determined HCN diffusional loss rate constant to provide an estimate for $k_{\mathrm{diff}}^{\mathrm{X}}$. This procedure should account for first-order species-dependent and geometrical effects.

C. Rate Constant Determination. For each experiment, temporal profiles of [NCO] were calculated by integrating the

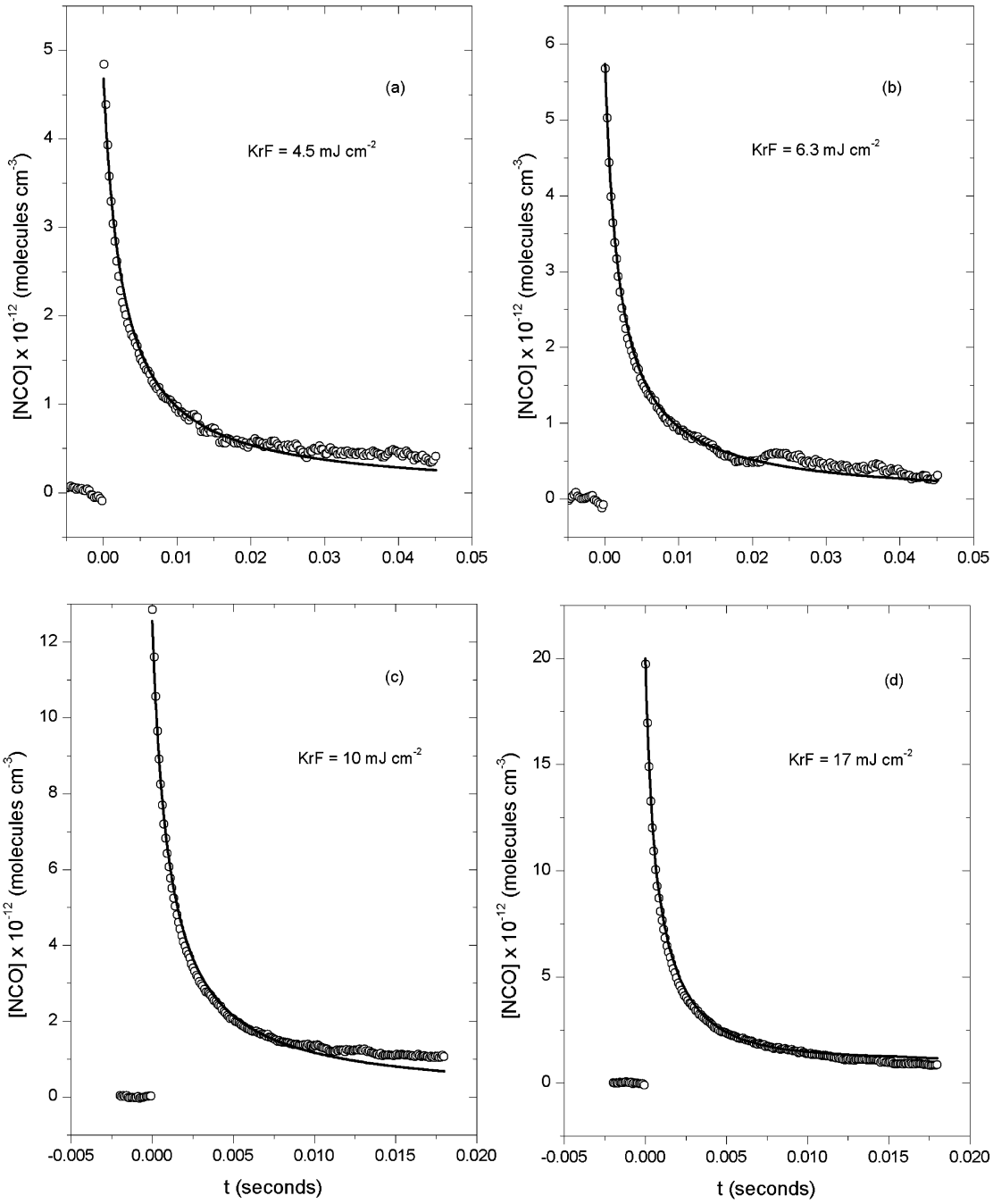

Figure 1. (a) Typical temporal concentration profile for NCO(00^10) in Ar at a photolysis laser fluence of 4.5 mJ cm.$^{-2}$ The solid curve is the best fit to the experimental data using a model outlined in section III.B. Both k_1 and k_5 were varied to minimize χ_{NCO}^2 as discussed in the text. (b), (c) and (d). Same as (a) except for photolysis laser fluences of 6.3, 10, and 17 mJ cm,$^{-2}$ respectively. The rate constants found for k_1 and k_5 were (a) 8.29×10^{-11} and 2.0×10^{-13}, (b) 8.28×10^{-11} and 1.3×10^{-13}, (c) 7.71×10^{-11} and 2.2×10^{-13}, and (d) 7.0×10^{-11} and 4.8×10^{-13} cm^3 molecules^{-1} s,$^{-1}$ respectively. The diffusion-rate constant, k_{diff}^{NCO} was calculated to be 42 s.$^{-1}$ The conditions of the experiment were [Ar] = 5.25 Torr and [ClNCO] = 0.0075 Torr, at a temperature of 293 K. For clarity, the data points in each panel are shown only every 10th point.

kinetic equations describing the reaction mechanism, reactions 1−7, and loss by diffusion for each species. The unknown rate constants, k_1 and k_5, were determined in a simple least-squares minimization procedure. For a fixed value of k_5 the value of k_1 was determined that minimized chi-squared, χ_{NCO}^2, i.e., the sum of the squares of the residuals between the calculated and experimental NCO concentration profiles. The value of k_5 was incremented by 1.0×10^{-13} cm^3 molecules^{-1} s^{-1} and a new optimized value of k_1 determined. This procedure was repeated until a global minimum in χ_{NCO}^2 was found.

Figure 1 shows four typical NCO temporal concentration profiles. The panels in Figure 1 were all recorded at the same reagent flow rates but with different photolysis laser fluences. Note that the initial concentration of NCO, $[NCO]_0$, increases linearly with laser fluence and the reaction time, $t_{1/2}$, scales approximately as the expected second-order behavior of $t_{1/2} = 1/(k_{\text{second order}}[NCO]_0)$, where $t_{1/2}$ is the time for the initial concentration to decay by one-half.

Figure 2 shows an enlarged Figure 1d. The solid curve shows the agreement between the experimental data and the values for k_1 and k_5 that produced a global minimum in χ_{NCO}^2. The dot−dot and dash−dot lines show the 68% confidence limits in the best-fit value. The long dash curve gives the optimized fit value for k_1 assuming that $k_5 = 0.0$. The calculated χ_{NCO}^2

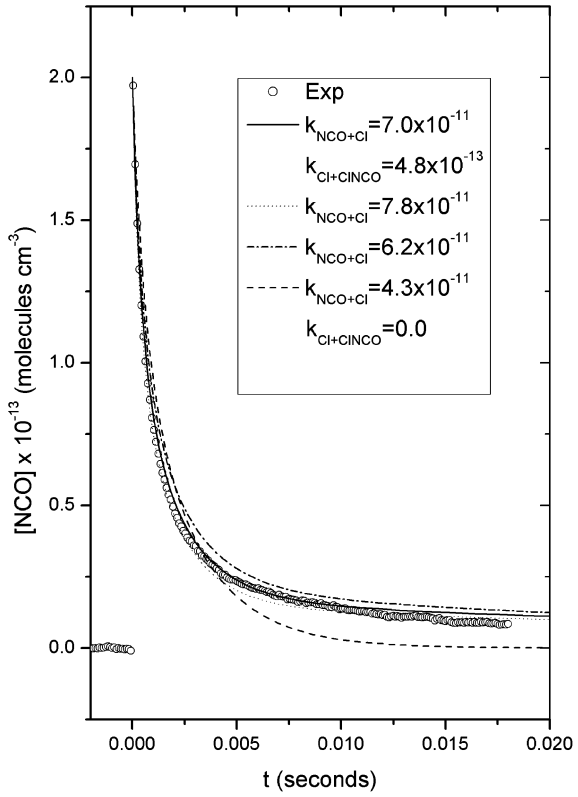

Figure 2. Expanded view of Figure 1d. The solid line is the fit to the experimental data resulting from the variation in k_1 and k_5 that minimized χ_{NCO}^2; see text and Figure 3. The dash and dash−dot curves show the 68% confidence limit in the goodness-of-fit for k_1 with k_5 set to 4.8×10^{-13} cm^3 molecules^{-1} s.$^{-1}$ The long dash curve shows the determination of k_1 neglecting reaction 5.

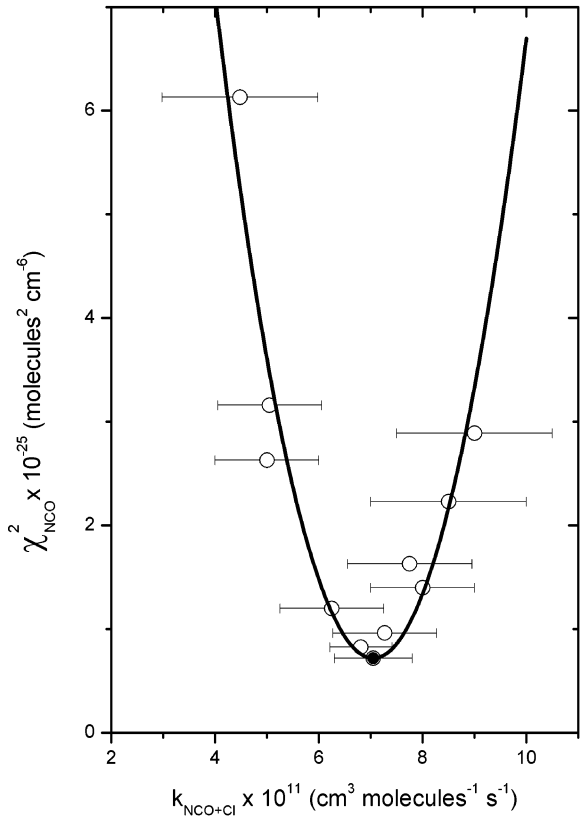

Figure 3. Variation in χ_{NCO}^2 as a function of k_1 for various values of k_5. The error bars show the 68% goodness-of-fit limits from the variation in k_1 that minimized χ_{NCO}^2. The solid point is the optimum value of k_1 determined using the value of k_5 at the minimum of χ_{NCO}^2. The solid line is a quadratic fit to the open circle calculations. The optimum values of k_1 and k_5 were found to be 7.0×10^{-11} and 4.8×10^{-13} cm^3 molecules^{-1} s,$^{-1}$ respectively.

for this case was 10 times larger than the best-fit case. As can be seen from Figure 2, $k_5 = 0.0$ gives a much poorer fit to the data, illustrating the importance of reaction 5 to the overall kinetics of NCO.

Figure 3 shows the variation in χ_{NCO}^2 as a function of the optimized value for k_1 at various values of k_5 for the analysis of the NCO profile shown in Figures 1d and 2. The k_5 values start at 0.0 and are incremented by 1.0×10^{-13} cm^3 molecule^{-1} s^{-1} at each point. The error bars give the 68% confidence limit range for the values k_1 found in the minimization procedure for χ_{NCO}^2. The solid dot is the global minimization for the optimum values for k_1 and k_5. The solid curve is a quadratic least-squares fit to the data and the dash line gives the 68% confidence limit for the best-fit optimization. If the reverse procedure is followed and k_5 is optimized for fixed values of k_1, similar values for k_5 and k_1 are found but the uncertainty in the optimized k_5 is generally larger than that shown in Figure 3 for k_1. This is a consequence of the greater sensitivity of the fit to the contribution of reaction 1 compared to reaction 5.

To determine the overall contribution to the removal of NCO made by a particular reaction, a reaction contribution factor analysis[28] was carried out for each reaction rate constant determination. The reaction contribution factor at time, t, for species i removed by reaction with species j, $RCF^i_j(t)$, is given by $RCF^i_j(t) = -k_{ij}[j][i]$, or produced in reaction between species l and m, $RCF^i_{lm}(t)$, is given by $RCF^i_{lm}(t) = k_{lm}[l][m]$. The corresponding integrated reaction contribution factor, $IRCF^i_{j/lm}$, from t = 0 to time t is the total flux of species i that is removed in reaction with j or produced in reaction between l and m, respectively, up to time t and is often called the reaction pathway contribution. A reaction pathway analysis gives a direct measure of the contribution a particular reaction makes to the overall reaction mechanism for reacting with or producing a given species. Such an analysis is shown in Figure 4 for the experiments at low $[NCO]_0$, Figure 1a, and high $[NCO]_0$, Figure 1d. The major difference between these two experiments is the larger contribution k^{NCO}_{diff} makes to the removal of NCO at low $[NCO]_0$. Reaction 5 contributes a similar amount to the production of NCO, on a relative basis, under the two experimental conditions, with $IRCF^{NCO}_{Cl\,ClNCO}$ approximately equal to 0.25 in both cases.

The results for the determination of k_1 as a function of Ar pressure are shown in Figure 5a and as a function of CF_4 pressure in Figure 5b. The dashed lines in Figure 5a,b are simple averages of each data set. The heavy lined error bar is the $\pm 1\sigma$ in the scatter of the data. As noted in the figure caption, each data point consists of the average of up to five data points obtained at the same concentration of carrier gas and ClNCO but different photolysis laser fluences, as illustrated in Figure 1. Although there might be a slight trend for k_1 to decrease with decreasing pressure, Figure 5a,b, the scatter in the data is sufficient to obscure any real pressure dependence and a simple average of the complete data set provides a good representation of the data. The value of k_1, for both Ar and CF_4 as carrier gas, was found to be $(6.9 \pm 1.3) \times 10^{-11}$ cm^3 molecules^{-1} s^{-1} at 293 ± 2 K.

Figure 6a,b shows the results for the determination of k_5 in both Ar and CF_4 carrier gases, respectively. Again, the dashed lines are the average of each data set. The combined average of both data sets gives k_5 to be $2.4 \pm 0.6 \times 10^{-13}$ cm^3

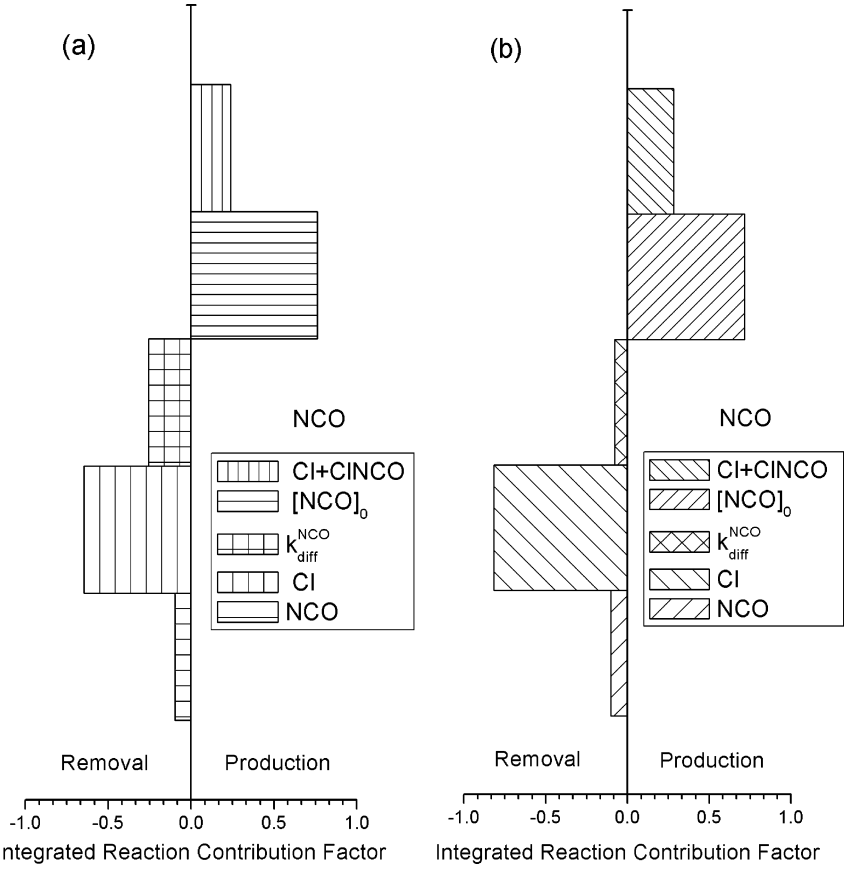

Figure 4. Integrated reaction contribution factors, $IRCF^{NCO}$, for the model calculations for the conditions in Figure 1a,d are shown. The $IRCF^{NCO}$ are expressed as a fraction of the total removal flux, negative, and total production flux, positive fractions. Photolysis is a production process. For (a) $[NCO]_0 = 5.00 \times 10^{12}$ and for (b) $[NCO]_0 = 1.98 \times 10^{13}$ molecules cm.$^{-3}$

molecule^{-1} s.$^{-1}$ As noted in section II, the concentration of ClNCO was not well determined because of the small flow of ClNCO admitted to the reaction chamber.

For other experiments involving ClNCO as a radical source being carried out in this laboratory, the values of k_1 and k_5 were needed at $T = 345$ K. These measurements were made in Ar only. Parts a and b of Figure 7 show the results for the determination of k_1 and k_5, respectively. The measurements were carried out at a temperature of 345 ± 3 K. Over the observed pressure range, k_1 was independent of pressure. At 345 K, the average value of k_1 was determined to be $(4.0 \pm 0.6) \times 10^{-11}$ cm^3 molecule^{-1} s^{-1}, and for k_5, the average value was $(1.9 \pm 1.0) \times 10^{-13}$ cm^3 molecule^{-1} s.$^{-1}$

IV. Discussion

A. Products of Reaction 1. In the present work, the products of reaction 1 were not identified experimentally but have been assumed to be $NCl(X^3\Sigma^-)$ + CO and not the recombination product, ClNCO. All other combinations of possible products, atom + triatom or diatom + diatom are substantially endothermic. There are several reasons for predicting that the dominant product channel for reaction 1 is the NCl + CO channel. The first is the work from Wategaonkar and Setser[21] on the analogous F + NCO reaction, and the second is an estimate of the Cl + NCO recombination rate constant using Troe's strong collision formulation of unimolecular reaction rate theory.[29] These are discussed in the following.

The rate constant for the F + NCO reaction[21] is a factor of 8 smaller than the determination of k_1 even though the F + NCO → $NF(X\ ^3\Sigma^-)$ + CO reaction is more exothermic by about 50 kJ mol^{-1} ($\Delta H_{r,0} = -89$ kJ mol^{-1} compared to −36 kJ mol^{-1}, for reaction 1). (The recent high level theoretical calculations[7] for the bond dissociation energies, D_0, of $NF(X^3\Sigma^-)$ and $NCl(X^3\Sigma^-)$ to be 315 ± 5.5 and 265 ± 5.5 kJ mol^{-1}, respectively, establishes the reaction enthalpies for these two reactions.) Du and Setser[30] detected the $NF(X^3\Sigma^-)$ product from the F + NCO reaction but did not quantify this observation. It should be noted that the reaction exothermicity for both systems is sufficiently small that the formation of the more energetic $NF/NCl(a^1\Delta)$ + CO channel is excluded at temperatures near 300 K. Wategaonkar and Setser[21] suggest that the F + NCO reaction likely occurs through the X^1A' PES, corresponding to a bound FNCO intermediate, followed by ISC to the FNCO-(a^3A'') PES, correlating to $NF(X^3\Sigma^-)$ + CO products. They argued the a^3A'' PES was likely repulsive so that direct reaction on this surface was unlikely. This mechanism is further strengthened by the observation that the quenching[31] of NF-$(a^1\Delta)$ by CO gives over 90% F + NCO; hence, redissociation over the X^1A' PES dominates over collisional stabilization to form FNCO. Indeed, this appears to be the case for Cl + NCO as well.

In general, the recombination of an atom and a radical composed of a few atoms to form a bound adduct is slow at low pressures because the recombination reaction is well in the falloff pressure region. However, k_1 was measured to be relatively fast, within a factor of 5 of a gas kinetic collision rate, and was found to be independent of the nature of the collision partner and pressure, Figure 5. It would be useful to have an estimate of the recombination of Cl + NCO to give the ClNCO recombination product.

The formulation of unimolecular reaction rate constants by Troe[29] provides a convenient mechanism for carrying out this

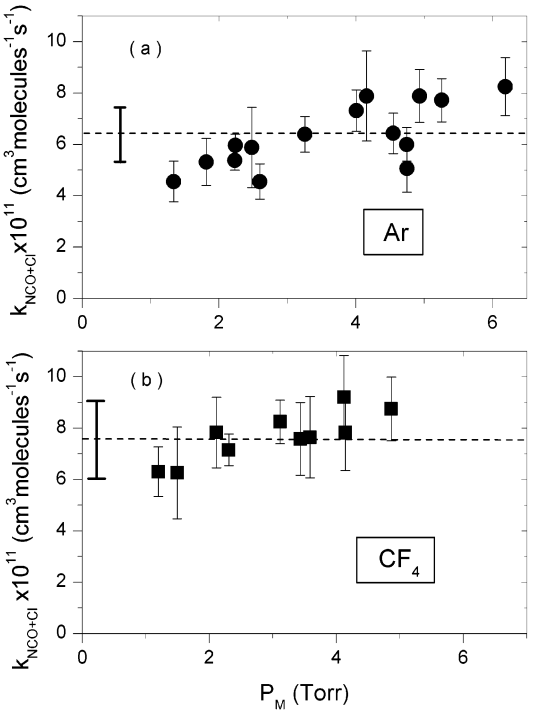

Figure 5. (a) Results for the determination of k_1 with Ar as carrier gas as a function of Ar pressure. The error bars are the scatter in several different measurements of k_1 with the same partial pressure of ClNCO but different $[NCO]_0$, as shown in Figure 1. The dashed line is the average of k_1 with Ar as carrier gas and the heavy error bar gives one standard deviation in the scatter of the data. (b) Same as (a) except the third body is a polyatomic molecule, CF_4. The determinations of k_1 were carried out at 293 ± 2 K. The value of k_1 was independent of pressure and the nature of the third body.

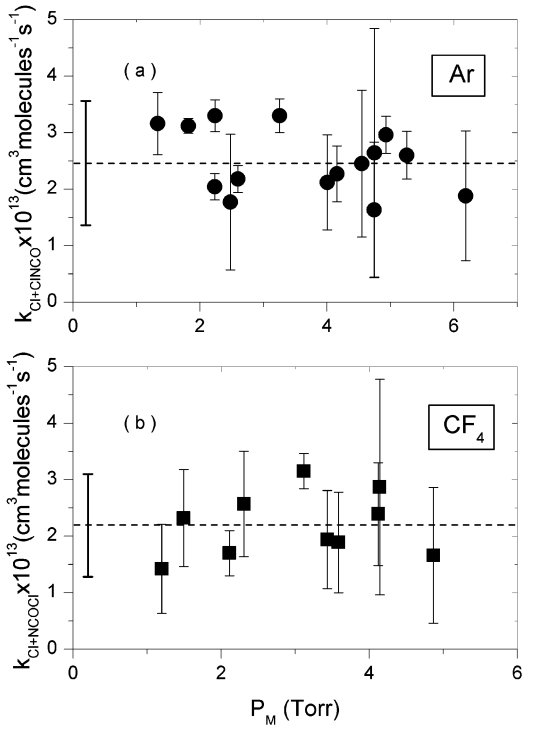

Figure 6. (a) Results for the determination of k_5 with Ar as carrier gas. k_5 was determined as illustrated in Figure 4; see text. The dashed line is the average of the data points and the heavy error bar gives the scatter in the data, $\pm 1\sigma$. (b) Same as (a) except CF_4 is the carrier gas.

analysis. This theory has been highly successful at reproducing a large number of experimental measurements of recombination

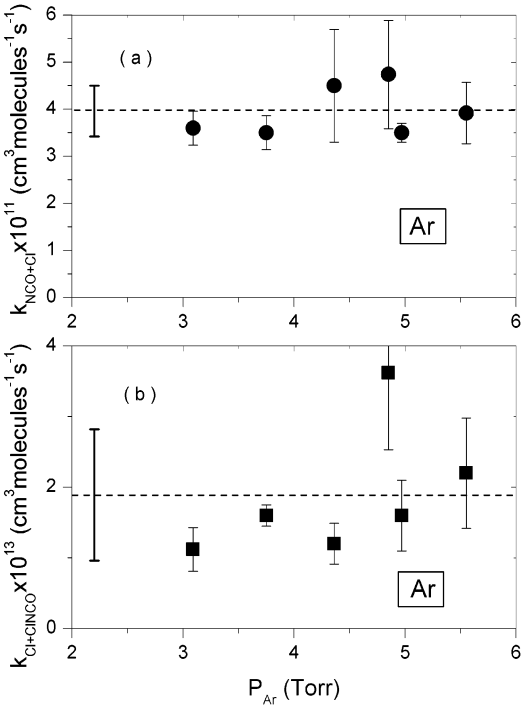

Figure 7. (a) Results for the determination of k_1 with Ar as carrier gas at a temperature of 345 ± 3 K. The dashed lined is the average of the data. (b) Results for the determination of k_5 with Ar carrier gas at a temperature of 345 ± 3 K.

TABLE 1: EA_X, D_0^{Cl-X}, and r_e^{Cl-X} of Elements and Compounds Bonding to a Cl Atom

species X Cl−X	electron affinity of X EA_X (eV)	equilib bond dist Cl−X r_e^{Cl-X}(Å)	dissociation energy Cl−X D_0^{Cl-X} (kJ mol^{-1})
−F	3.4012[a]	1.6281[a]	252[b]
−Cl	3.614[a]	1.988[a]	239.2[b]
−N	−0.0725[a]	1.6107[c]	265.4[c]
−NCl	-	1.71[d]	(152)[d]
−NO	0.026[a]	1.975[e]	156[b]
$-NO_2$	2.273[a]	1.840[f]	138[b]
$-N_3$	2.762[g]	1.745[h]	180[i]
−NCO	3.609[j]	1.705[k]	195[l]

[a] Reference 35. [b] Reference 40. [c] Reference 7, D_0^{Cl-N} corrected for ZPE. [d] Reference 36. Theoretical calculation of structure and atomization energy of NCl_2. [e] Reference 37. [f] Reference 38. [g] Reference 34. [h] Reference 39. [i] Reference 41. [j] Reference 33. [k] Reference 31. [l] Calculated using eq E3.

rate constants.[32] The recombination rate constant for two radicals forming an adduct, k_{rec}, is related to the unimolecular dissociation rate constant of the adduct back to the initial radicals, k_{diss} through the equilibrium constant, K_{eq}, i.e., $k_{rec} = k_{diss}/K_{eq}$. For a PES without an activation barrier, the low-pressure strong-collision expression for k_{diss} is given as[29]

$$k_{diss}^{sc} = Z_{LJ}\rho_{vib}(E_0)\frac{kT}{Q_{vib}}e^{-E_0/kT}F_{anh}F_E F_{rot}F_{corr} \qquad \text{(E2)}$$

where Z_{LJ} is the Lennard-Jones collision rate constant, $\rho_{vib}(E_0)$ is the Witten-Rabinovitch vibrational density of states calculated at the dissociation energy E_0, k is Boltzmann's constant, and the terms F_{anh}, F_E, and F_{rot} are corrections to the density of states calculation. The term F_{corr} corresponds to a correction factor for coupling between the different degrees of freedom and is assumed to be small, i.e., $F_{corr} = 1.0$. The parameters

necessary to calculate the Lennard-Jones collision rate constant for Ar, ClNCO collisions were taken from estimates of similar collision partners.[27] The parameters to calculate the density of states and the correction factors were taken from spectroscopic measurements on ClNCO.[33,34]

Unfortunately, the calculation of k_{diss} is most sensitive to the value of the bond dissociation energy, E_0, of ClNCO, for which there appears to be no available data. Table 1 lists properties of Cl−X species, primarily involving Cl−N bonds, that could be used to estimate bond energies such as electron affinities,[35−37] EA_X, of the atom or radical, X, bonding to the Cl atom, equilibrium bond lengths,[38−41] r_e^{Cl-X}, and bond dissociation energies[42,43] for the Cl−X bond, D_0^{Cl-X}. As can be seen from Table 1, there appears to be little correlation between D_0 and the EA of the bonding species, X. However, as noted by Johnston and Parr in the formulation of the BEBO theory for H atom transfer reactions,[44] Paulings relationships between bond length and bond order and the relationship between bond energy and bond order can be used to estimate bond energy as a function of bond length. The bond energy and bond length of a pure single bond and the binding energy and bond length for the corresponding inert gas compound (Ne−Ar for N−Cl bonding) was taken from Johnson.[45] D_0^{ClNCO} is estimated from the equation

$$D_0^{ClNCO} = D_0^{NCl} \exp[p(r_e^{NCl} - r_e^{Cl-NCO})] \qquad \text{(E3)}$$

where p is calculated from the properties of the NCl single bond and the corresponding inert gas compound to be 0.8721. Using equation E3, D_0^{ClNCO} was calculated to be 195 kJ mol^{-1}. As can be seen from Table 1, this estimate for D_0^{ClNCO} appears reasonable compared to other D_0 values for Cl−N bonds in a variety of compounds.

The calculated value for k_{rec}, according to eq E2, was 9.0×10^{-30} cm^6 molecules^2 s^{-1} at a temperature of 293 K. At an Ar pressure of 5.0 Torr, the bimolecular rate, k_{rec}[Ar], would be 1.5×10^{-12} cm^3 molecules^{-1} s^{-1}. This rate constant is about 50 times slower than the measured value of k_1, Figure 5. If D_0^{ClNCO} is increased to 230 kJ mol^{-1}, slightly less than the $D_0^{Cl_2}$, k_{rec} is only increased by a factor of 3 so that the recombination rate in Ar would still be a factor of 16 slower than the observed k_1. The strong collision k_{rec} does not take into account falloff effects and so is an upper bound to the true recombination rate constant. From this and the conclusions of Wategaonkar and Setser[21] on the product channel for the analogous F + NCO system, it is concluded that the products must be NCl(X $^3\Sigma^-$) + CO and the formation of ClNCO is a minor channel.

B. Comparison of N_3 + Cl and NCO + Cl. As noted in the Introduction, the N_3 and NCO radicals are isoelectronic, and hence, have similar properties. Both radicals are linear with $^2\Pi$ ground states, and hence, subject to the Renner−Teller effect.[46] The spin−orbit parameters of both species are also similar with values of −71.3 and −95.6 cm,$^{-1}$ for N_3 and NCO, respectively.[47,48] The ground electronic state of both radicals correlates to an excited N(^{2}D) atom and a ground state $^1\Sigma^+$ diatom fragment so the dissociation pathway leading to a ground-state N(^{4}S) atom and an $^1\Sigma^+$ diatom partner results from ISC. As a result, the N−diatom bond is thermodynamically weak for both radicals. In fact, the N_3 radical is actually a metastable species. The largest difference between N_3 and NCO is the much larger heat of formation[49] of N_3, $\Delta H_{f,0}^0(N_3) = 476 \pm 9.6$ kJ mol^{-1} compared[6] to NCO, $\Delta H_{f,0}^0(NCO) = 128 \pm 0.8$ kJ mol^{-1}. Thus, reactions involving the N_3 radical are much more energetic than those involving NCO.

The $\Delta H_{r,0}^0$ for the Cl + N_3 → NCl($X^3\Sigma^-$) + N_2 reaction is -270 ± 15 kJ mol^{-1} whereas $\Delta H_{r,0}^0$ for reaction 1 is only -36 ± 6 kJ mol^{-1}. Unlike the Cl + NCO reaction, the Cl + N_3 reaction has sufficient energy to directly populate NCl($a^1\Delta$). In fact, the Cl + N_3 reaction is used as source of electronically excited NCl($a^1\Delta$) to chemically activate an I atom laser.[50] Modeling studies[51,52] of the production and quenching of NCl($a^1\Delta$) in flowing F/HN_3/Cl mixtures indicate that the branching fraction into the NCl($a^1\Delta$) state is greater than 0.7 for the Cl + N_3 reaction. Although there is some discrepancy as to the value of the reaction rate constant for the Cl + N_3 reaction, Hewett and Setser[53] provide the most direct determination and give a value of $2.1^{+1.0}_{-0.6} \times 10^{-11}$ cm^3 molecules^{-1} s^{-1} at 300 K. At this same temperature, the value of k_1 is a factor of 3.5 larger than the rate constant for Cl + N_3 even though reaction 1 is exothermic by only 36 kJ mol^{-1}. This appears to be a general trend between the chemical kinetics of NCO and N_3 radicals reacting with other radical species or unsaturated molecules. The rate constants for NCO reactions are faster even though the reaction exothermicity is smaller.

Further insight into the reaction dynamics of the Cl + N_3 system is obtained by recent theoretical calculations of Chen and Huang at the CASPT2 level of theory.[54] These calculations clearly show that the reaction occurs over the $ClN_3(X^1A')$ well. The NCl($a^1\Delta$) + N_2 products are formed after passage over a transition state that is energetically very close to the Cl + N_3 asymptote. At 300 K, the formation of the NCl($X^3\Sigma^-$) + N_2 products cannot occur directly from the Cl + N_3 reactants through reaction on the lowest lying triplet PES because the initial interaction is repulsive with a calculated barrier of 18 kJ mol^{-1}. The crossing seam between the singlet and triplet surfaces occurs past the transition state to the NCl($a^1\Delta$) + N_2 products and is only crossed while NCl and N_2 are separating. Under such circumstances, the ISC crossing rate will be small, and the formation of the NCl($a^1\Delta$) + N_2 will dominate, as observed experimentally. The rate constant for NCl($a^1\Delta$) + N_2 formation is substantially smaller than the adduct formation rate because redissociation back to Cl + N_3 reactants dominates over passage through an energetic transition state on the singlet PES.

The reaction dynamics for the Cl + NCO system should be similar to those for the Cl + N_3 system just discussed except that singlet state products are energetically forbidden. As outlined in the section IV.A, at the pressures of the present experiment, the recombination of Cl + NCO to form singlet products, $ClNCO(X^1A')$, does not compete with the formation of the triplet, NCl($X^3\Sigma^-$) + CO, products. As in the Cl + N_3 reaction, the reaction Cl + NCO cannot proceed directly over the lowest energy triplet PES because the initial interaction between Cl and NCO is likely repulsive. Further evidence for this conclusion comes from several sources. Recent theoretical calculations on the related F + NCO system,[55] using density functional theory to investigate the FNCO(a^3A'') surface, shows that there are significant barriers to the direct formation of the NF($X^3\Sigma^-$) + CO products. Formation of an NCFO adduct is possible on the triplet PES, but there is a 160 kJ mol^{-1} barrier leading to the NF($X^3\Sigma^-$) + CO asymptote from this adduct. For the four systems: H + NCO,[56] F + NCO,[55] F + N_3,[57] and Cl + N_3,[54] the initial interaction of the atom with the radical on the triplet PES is repulsive, preventing direct formation of triplet surface products by this interaction. As concluded by Wategaonkar and Setser,[21] the Cl + NCO system (reaction 1) must proceed over the singlet $ClNCO(X^2A')$ PES, and the formation of the NCl($X^3\Sigma^-$) + CO products occurs by ISC. The formation of an energetic $ClNCO(X^1A')$ adduct likely

facilitates the ISC by allowing the system to sample the crossing seam between the singlet and triplet surfaces multiple times. This situation has been described many years ago in the classic paper by Tully[58] on the quenching of $O(^1D)$ by N_2.

C. Temperature Dependence k_1. The temperature dependence of k_1 was not fully investigated in the present work; however, the near factor of 2 decrease in k_1 from 293 to 345 K is surprising. It implies a temperature dependence of k_1 on $T^{-3.34}$. Such a steep dependence on temperature of a reaction rate constant based on adduct formation cannot simply arise from an expected decrease in adduct formation rate with increasing temperature. It may indicate a delicate competition between redissociation of the initial complex and ISC rate processes or, most likely, the temperature dependence is exaggerated because of the small range over which it was determined, and results largely from experimental scatter.

D. Comparison of Cl + ClN_3 and Cl + ClNCO. Brunning and Clyne[59] have measured the reaction rate constant for Cl + $ClN_3 \rightarrow Cl_2 + N_3$ to be $(1.8 \pm 0.3) \times 10^{-12}$ cm^3 molecules^{-1} s^{-1} at 295 K. This reaction is analogous to the Cl + ClNCO reaction and k_5 was found to be $(2.4 \pm 0.6) \times 10^{-13}$ cm^3 molecules^{-1} s^{-1} at 293 K, Figure 6. Thus, the reaction rate constant for Cl + ClN_3 is almost an order of magnitude faster than that for the Cl + ClNCO system. The $\Delta H^0_{r,0}$ for the Cl + ClN_3 reaction is calculated to be -59 kJ mol^{-1}. (The $\Delta H^0_{f,0}$ (ClN_3) can be calculated to be 415 kJ mol^{-1}, using the recent measurement[43] of the $NCl(X^3\Sigma^-) + N_2$ threshold energy of 89.7 kJ mol^{-1} following the 203 nm photodissociation of ClN_3.) Using the estimate of the bond dissociation energy for the Cl−NCO molecule given in Table 1, the $\Delta H^0_{r,0}$ for Cl + ClNCO is estimated to be -44 ± 20 kJ mol^{-1}. The difference in reaction rate constants between these two systems must be driven by the slightly stronger Cl−N bond in ClNCO and, hence, a slightly larger activation energy in this system. The structures of the transition states for both reactions are likely similar so that entropic effects between these systems would be expected to be small.

E. Estimated Uncertainties in k_1 and k_5. The determination of k_1 requires the [NCO] and the [Cl] to be known, and hence, the uncertainty in the concentration measurement directly affects the uncertainty in the rate constant. As noted in section III.A, the σ_{pk} for the NCO(10^10) $P_{e/f}$(12.5) transition was determined[16] with an uncertainty of ±8%. This introduces an uncertainty of ±8% in the determination of k_1.

The reaction mechanism consists of five chemical reactions and loss by diffusion. The $IRCF_i^{NCO}$ analysis illustrated in Figure 4 is representative of the total reaction flux that passes through each reaction step in the overall mechanism that affects the [NCO]. As a first-order approximation, the uncertainty in a rate constant for species i reacting with NCO times the $IRCF_i^{NCO}$ provides an estimate of the contribution the uncertainty in this rate constant makes to the uncertainty in the overall [NCO], hence the uncertainty in determining k_1. There are only three reactions directly affecting the removal of NCO, k_1, k_3, and k_{diff}^{NCO}. The uncertainty[21] in k_3 is ±40% and the uncertainty in k_{diff}^{NCO} is estimated to be ±20%. As illustrated in Figure 4, $IRCF_{NCO}^{NCO}$ was 10% and $IRCF_{diff}^{NCO}$ was 25%; thus, the uncertainty in the rate constants for these processes contributes about ±4% and ±5%, respectively, to the overall uncertainty in the determination of k_1. The only reaction contributing to the production of NCO is reaction 5, and as can be seen from Figure 4, reaction 5 contributes about 25% to the total NCO production. The uncertainty in k_5 is taken to be the experimental scatter of ±25%, Figures6 and 7b; thus, this process contributes an overall uncertainty of about ±6% to k_1. The considerations of the $IRCF_i^{NCO}$ flux analysis indicates that the uncertainty in the rate constants influencing the NCO concentration can be up to ±15%, over the broad range of conditions of the experiment (±4% + ±5% + ±6%).

Similar considerations can be applied to the influence of the uncertainties in the model rate processes on the [Cl]. There are only two processes that have not been considered, the production of Cl atoms by reaction 4 and their loss by diffusion. The uncertainty[22] in k_4 is ±22% whereas the maximum $IRCF_{NClNCl}^{Cl}$, which occurs at the largest initial [NCO], is taken to be ±40% for the complete data set. Thus the uncertainty in k_4 contributes an uncertainty of ±9% to k_1. The uncertainty in k_{diff}^{Cl} is taken to be the same as for k_{diff}^{NCO}, ±20%. Because Cl atoms are removed by reaction with ClNCO, $IRCF_{diff}^{Cl}$ is only about half that for NCO and contributes about 15% to removal of Cl atoms. Thus, the uncertainty in k_{diff}^{Cl} was estimated to contribute ±3% to the uncertainty in k_1. The total uncertainty in the [Cl] contributes ±(9%+3%) or ±12% to the overall uncertainty in k_1.

The procedure to determine k_1 is illustrated in Figure 2 and more completely in Figure 3. Generally, the determination of k_1 by the χ_{NCO}^2 minimization procedure returned an uncertainty of about ±10% at the 68% goodness-of-fit level, slightly less than the overall scatter for the complete data set of ±20%. Assuming no systematic errors, these two sources of error should be comparable, as indeed, they are, and there is no additional error factor due to the fitting procedure other than the scatter in the data.

The overall experimental uncertainty in determining k_1 can be estimated to be the sum of the following: the scatter in the complete data set, ±20%, the uncertainty in determining σ_{pk}, ±8%, and the sum of the contributions of the rate constant uncertainties in the model from both NCO, ±15%, and Cl reactions, ±12%. Thus, the overall uncertainty in k_1 is estimated to be ±55%, including both random and systematic errors.

Similar considerations can be made to the overall uncertainty in determining k_5 except for the addition uncertainty in determining the [ClNCO]. As noted in section II, the [ClNCO] was uncertain to ±20%. The factors influencing the uncertainty in the determination of k_5 are the uncertainty in the measurement of the initial $[Cl]_0$, i.e., the uncertainty in the NCO absorption coefficient, ±8%, and the uncertainty in the Cl atom concentration due to production by reaction 4 and loss by diffusion. As noted above, these two processes contributed a maximum uncertainty to [Cl] of ±12%. Undoubtedly, some of the scatter in determining k_5, as illustrated in Figure 3, results from the uncertainty in measuring the [ClNCO]; however, these two effects cannot be separated and are simply added together.

The overall uncertainty in determining k_5 is the scatter in the measurements, ±25%, the uncertainty in determining the [Cl], ±8%, the uncertainty in determining the [ClNCO], ± 20%, and the uncertainty in the contribution of reaction 4 and diffusion to the [Cl], ±12%. Thus, k_5 is estimated to be determined with an uncertainty of ±65%, including both random and systematic errors.

V. Summary

The rate constant for the Cl + NCO reaction was measured to be $(6.9 \pm 3.8) \times 10^{-11}$ at 293 ± 2 K and $(4.0 \pm 2.2) \times 10^{-11}$ cm^3 molecules^{-1} s^{-1} at 345 ± 3 K, where the uncertainty includes both random and systematic errors. The rate constant was found to be independent of pressure and the nature of the third-body collision partner, either Ar or CF_4. The products of

the reaction were argued to be $NCl(^3\Sigma^-) + CO$, correlating to the lowest energetic triplet (a^3A'') PES. The calculated strong collision recombination rate constant to form ground singlet $ClNCO(X^1A')$ products was found to be 50 times smaller than the measurement of k_1. Insight into the reaction dynamics for Cl + NCO was provided by comparisons with analogous systems, F + NCO and Cl + N_3. The reaction proceeds by the formation of an energized $ClNCO(X^1A')$ adduct, and formation of the $NCl(X^3\Sigma^-)$ + CO products results from ISC. There is competition between redissociation of the energized adduct back to reactants and the ISC process.

The reaction rate constant for the Cl + ClNCO → Cl_2 + NCO was also measured and found to be $(2.4 \pm 1.6) \times 10^{-13}$ at 293 ± 2 K and $(1.9 \pm 1.2) \times 10^{-13}$ at 345 ± 3 K, where the uncertainty includes both random and systematic errors.

Acknowledgment. This work was supported by the U.S. Department of Energy, Office of Basic Energy Sciences, Division of Chemical Sciences, Geosciences, and Biosciences, under contract No. W-31-109-ENG-38.

References and Notes

(1) Lissianski, V. V.; Zamansky, V. M.; Gardiner, W. C., Jr. *In Gas-Phase Combustion Chemistry*; Gardiner, W. C., Jr., Ed.; Springer-Verlag: New York, 2000; p 46.
(2) Miller, J. A.; Bowman, C. T. *Prog. Energy Combust. Sci.* **1989**, *15*, 287.
(3) Pilling, M. J.; Stocker, D. W. *Annu. Rep. Prog. Chem., Sect. C* **1999**, *95*, 277.
(4) Smith, I. W. M. *Int. J. Chem. Kinet.* **1984**, *16*, 423.
(5) Yarkony, D. R. *J. Phys. Chem. A* **2001**, *105*, 6277.
(6) Schuurman, M. S.; Muir, S. R.; Allen, W. D.; Schaefer, H. F., III. *J. Chem. Phys.* **2004**, *120*, 11586.
(7) Xantheas, S. S.; Dunning, T. H., Jr.; Mavridis, A. *J. Chem. Phys.* **1997**, *106*, 3280.
(8) Henshaw, T. L.; Manke, G. C.; Madden, T. J.; Berman, G. D.; Hager, G. D. *Chem. Phys. Lett.* **2000**, *325*, 537.
(9) Decker, B. K.; Macdonald, R. G. *J. Phys. Chem. A* **2001**, *105*, 6817.
(10) Nachbaur, E.; Gottardi, W. *Monatsh. Chem.* **1965**, *97*, 115.
(11) Bell, D. D.; Coombe, R. D. *J. Chem. Phys.* **1985**, *82*, 1317.
(12) Kroto, H. W. *Molecular Rotational Spectra*; Dover: New York, 1992.
(13) Wright, S. A.; Dagdigian, P. J. *J. Chem. Phys.* **1995**, *103*, 6479.
(14) Astbury, C. J.; Hancock, G.; McKendrick, K. G. *J. Chem. Soc., Faraday Trans.* **1993**, *89*, 405.
(15) Macdonald, R. G.; Liu, K. *J. Chem. Phys.* **1993**, *98*, 3716.
(16) Decker, B. K.; Macdonald, R. G. Manuscript in preparation.
(17) Gao, Y.; Macdonald, R. G. *J. Phys. Chem. A* **2003**, *107*, 4625.
(18) Patel-Misra, D.; Sauder, D. G.; Dagdigian, P. J. *J. Chem. Phys.* **1990**, *93*, 5448.
(19) Gilbert, J. V.; Coombe, R. D. *J. Chem. Phys.* **1988**, *89*, 4082.
(20) Gao, Y.; Macdonald, R. G. Manuscript in preparation.
(21) Wategaonkar, S.; Setser, D. W. *J. Phys. Chem.* **1993**, *97*, 10028.
(22) Clyne, M. A. A.; MacRobert, A. J. *J. Chem. Soc., Faraday Trans. 2* **1983**, *79*, 283.
(23) Cheah, C. T.; Clyne, M. A. A.; Whitefield, P. D. *J. Chem. Soc., Faraday Trans. 2* **1980**, *76*, 711.
(24) Weng, C.-J.; Ho, T.-I.; Su, T.-M. *J. Phys. Chem.* **1987**, *91*, 5235.
(25) Reid, R. C.; Prausnitz, J. M.; Poling, B. E. *The Properties of Gases and Liquids*; McGraw-Hill: New York, 1989.
(26) McDaniel, E. W. *Collision Phenomena in Ionized Gases*; Wiley: New York, 1964.
(27) Svehla, R. A. *NASA Technol. Rep. R-132*; Lewis Research Center: Cleveland, OH, 1962.
(28) Warnatz, J.; Maas, U.; Dibble, R. W. *Combustion: Physical and Chemical Fundamentals, Modeling and Simulation, Experiments, Pollution Formation*; Springer: Berlin, 1995.
(29) Troe, J. *J. Chem. Phys.* **1977**, *66*, 4758.
(30) Du, K.-Y.; Setser, D. W. *Chem. Phys. Lett.* **1988**, *153*, 393.
(31) Wategaonkar, S.; Du, K.-Y.; Setser, D. W. *Chem. Phys. Lett.* **1991**, *99*, 586.
(32) Patrick, R.; Golden, D. M. *Int. J. Chem. Kinet.* **1983**, *15*, 1189.
(33) Hocking, W. H.; Gerry, M. C. L. *J. Mol. Spectrosc.* **1972**, *42*, 547.
(34) Devore, T. C. *J. Mol. Structure* **1987**, *162*, 287.
(35) Bradforth, S. E.; Kim, E. H.; Arnold, D. W.; Neumark, D. M. *J. Chem. Phys.* **1993**, *98*, 800.
(36) Illenbeger, I.; Commita, P. B.; Brauman, J. I.; Fenzlaff, H.-P.; Heni, M.; Heinrich, N.; Koch, W.; Frenking, G. *Ber. Bunsen-Ges.-Phys. Chem. Chem. Phy.* **1985**, *89*, 1026.
(37) Linstrom, P. J.; Mallard, W. G. Eds; *NIST Chemistry WebBook, NIST Standard Reference Database Number 69*; National Institute of Standards and Technology: Gaithersburg, MD, 2003 (http://webbook.nist.gov).
(38) Papakondylis, A.; Mavfidis, A.; Metroppoulos, A. *J. Phys. Chem.* **1995**, *99*, 10759.
(39) Cazzoli, G.; Esposti, C. D.; Palmieri, P.; Simone, S. *J. Mol. Spectrosc.* **1983**, *97*, 165.
(40) Lee, T. J. *J. Phys. Chem.* **1994**, *98*, 111.
(41) Cook, R. L.; Gerry, M. C. L. *J. Chem. Phys.* **1970**, *53*, 2525.
(42) Atkinson, R.; Baulch, D. L.; Cox, R. A.; Hampson, R. F.; Kerr, J. A.; Troe, J. *J. Phys. Chem. Ref. Data* **1992**, *21*, 1125.
(43) Hansen, N.; Wodtke, A. M.; Komissarov, A. V.; Heaven, M. C. *Chem. Phys. Lett.* **2003**, *368*, 568.
(44) Johnson, H. S.; Parr, C. *J. Am. Chem. Soc.* **1963**, *85*, 2544.
(45) Johnston, H. S. *Gas-Phase Reaction Rate Theory*; Ronald Press: New York, 1966.
(46) Herzberg, G.; *Molecular Spectra and Molecular Structure III. Electronic Spectra and Electronic structure of Polyatomic Molecules*; Van Nostrand Reinhold: New York, 1966.
(47) Douglas, A. E.; Jones, W. J. *Can. J. Phys.* **1965**, *43*, 2216.
(48) Bolman, P. S. H.; Brown, J. M.; Carrington, F. R. S.; Kopp, I.; Ramsay, D. A. *Proc. R. Soc. London A* **1975**, *343*, 17.
(49) Continetti, R. E.; Cyr, D. R.; Osborn, D. L.; Leahy, D. J.; Neumark, D. M. *J. Chem. Phys.* **1993**, *99*, 2616.
(50) Manke, G. C., II; Cooper, C. B.; Dass, S. C.; Madden, T. J.; Hager, G. D. *IEEE J. Quantum Electron.* **2003**, *39*, 995.
(51) Manke, G. C., II; Setser, D. W. *J. Phys. Chem.* **1998**, *102*, 7257.
(52) Henshaw, T. L.; Herrera, S. D.; Schile, L. A. *J. Phys. Chem.* **1998**, *102*, 6239.
(53) Hewett, K. B.; Setser, D. W. *J. Phys. Chem.* **1998**, *102*, 6274.
(54) Chen, B.-Z.; Huang, M.-B. *Chem. Phys. Lett.* **2003**, *373*, 124.
(55) Zhou, Z.-Y.; Guo, L.; Gao, H.-W. *Int. J. Chem. Kinet.* **2003**, *35*, 52.
(56) Mebel, A. M.; Luna, A.; Lin, M. C.; Morokuma, K. *J. Chem. Phys.* **1996**, *105*, 6439.
(57) Habdas, J.; Wategaonkar, S.; Setser, D. W. *J. Phys. Chem.* **1987**, *91*, 451.
(58) Tully, J. C. *J. Chem. Phys.* **1974**, *61*, 61.
(59) Brunning, J.; Clynne, M. A. A.; *Chem Phys. Lett.* **1984**, *106*, 337.